Published in final edited form as:
Inorg Chem. 2012 March 5; 51(5): 2841–2851. doi:10.1021/ic2019296.

Dioxygen reactivity of new bispidine-copper complexes

Peter Comba[a], **Christina Haaf**[a], **Stefan Helmle**[a], **Kenneth D. Karlin**[b], **Shanthi Pandian**[a], and **Arkadius Waleska**[a]

Peter Comba: peter.comba@aci.uni-heidelberg.de

[a]Universität Heidelberg, Anorganisch-Chemisches Institut, INF 270, D-69120 Heidelberg, Germany, Fax: +49-6226-546617

[b]Department of Chemistry, The Johns Hopkins University, Baltimore, Maryland 21218, USA

Abstract

The reactivity of copper complexes of three different 2nd generation bispidine-based ligands (bispidine = 3,7-diazabicyclo[3.3.1]nonane; mono- and bis-tetradentate; exclusively tertiary amine donors) with dioxygen [(reversible) binding of dioxygen by copper(I)] is reported. The UV-vis, electrospray ionization mass spectra (ESI-MS), electron paramagnetic resonance (EPR) and vibrational spectra (resonance Raman,rR) of the dioxygen adducts indicate that, depending on the ligand and reaction conditions, several different species (mono- and dinuclear, superoxo, peroxo and hydroperoxo), partially in equilibrium with each other, are formed. Minor changes in the ligand structure and/or experimental conditions (solvent, temperature, relative concentrations) allow switching between the different forms. With one of the ligands, an end-on-peroxo-dicopper(II) and a mononuclear copper(II)-hydroperoxo complex could be characterized. With another ligand, reversible dioxygen binding was observed, leading to a meta-stable copper(II)-superoxo complex, and the amount of dioxygen involved in the reversible binding to Cu^{I} was determined quantitatively. The mechanism of dioxygen binding as well as the preference of each of the three ligands for a particular dioxygen adduct is discussed on the basis of a computational (DFT) analysis.

Introduction

A broad range of aerobic oxidation reactions are catalyzed by copper enzymes and low molecular weight model complexes. A number of catalytically relevant mono- and dinuclear $[CuO_2]^{n+}$ and $[Cu_2O_2]^{2+}$ species have been identified and thoroughly studied spectroscopically, structurally, with computational methods and in terms of their reactivity. Apart from the various types of oxygen adducts (dioxygen, superoxo, peroxo, oxo) and copper in different oxidation states (Cu^{I}, Cu^{II}, Cu^{III}), it is particularly the $[Cu_2O_2]^{2+}$ core which has attracted much attention, specifically in terms of the various possible isomers (bis-μ-oxo, μ-η^2:η^2-peroxo, *trans*-μ-1,2-peroxo).[1–9] The suitability of copper for the activation of dioxygen derives from the favorable redox potentials, tunable over a broad range by the coordination geometry and donor sets. A large variety of ligand systems are known and serve as a valuable basis for biomimetic copper chemistry;[4–8, 10, 11] the reactivity and stability ranges depend on the geometry enforced and the donor set provided by the

Correspondence to: Peter Comba, peter.comba@aci.uni-heidelberg.de; Kenneth D. Karlin.

Supporting Information

Additional time-resolved electronic spectra, the experiment showing the O_2 recovery from $[Cu^{II}(L^2)O_2]^{+}$, EPR spectra of $[Cu^{II}(L^1)(NCMe)]^{2+}$ and $[Cu^{II}(L^2)(OH)]^{+}$, CV diagrams of $[Cu^{II}(L^1)(NCMe)]^{2+}$, $[Cu^{II}(L^2)(OH)]^{+}$ and $[Cu^{II}{}_2(L^3)(NCMe)_2]^{4+}$, an ESI-MS experiment to show the ligand oxidation of $[Cu_2{}^{I}(L^3)(solvent)]^{n+}$ upon oxygenation, and details of the DFT calculations are given as Supporting Information.

ligand. Structure–activity correlations have been established and are used to modulate the properties of the copper center in order to establish mimics for specific natural systems for electron transfer, dioxygen transport, oxidation or oxygenation reactivity.

The copper-dioxygen chemistry of a range of bi-, tri- and tetradentate amine-, imine- and pyridine-containing ligands with the, in the area of copper-based oxygen activation, well established tmpa (tmpa = tris-(methylpyridine)amine), tacn (tacn = 1,4,7-triazacyclononane), hydro-trispyrazolylborate, tren (tren = tris-ethylaminoethane), β-diketiminate ligands and their derivatives, in particular also the “superbasic” tetramethylguanidino-substituted amine ligands, has lead to exciting discoveries, and this has been reviewed extensively.[9, 11, 12] The transition metal coordination chemistry of a large range of tetra-, penta- and hexadentate bispidine ligands (bispidine = 3,7-diazabicyclo[3.3.1]nonane) has started to attract the attention of coordination chemists less than a decade ago, although the first bispidine derivatives have been described by Mannich.[13–16] The 1st generation bispidine ligands have mixed aliphatic/aromatic nitrogen donor sets and enforce distorted *cis*-octahedral coordination geometries; the corresponding copper complexes have been shown to provide interesting enzyme models and efficient catalysts.[17–22] Of particular interest for the copper-dioxygen chemistry is the fact that the enforced square-pyramidal geometry with an axial amine and in-plane coordination of the substrate (i.e. the dioxygen-derived ligand) leads to an unusual stability of the peroxo complexes,[17, 18, 20, 21] specific reactivities[19, 23] and interesting spectroscopic properties.[21, 24]

In the recently introduced 2nd generation bispidine ligands with pure aliphatic donor sets,[16, 25] very different, i.e., distorted trigonal structures (trigonal bipyramidal or trigonal prismatic) are enforced, and this has important consequences for the electronic properties and therefore also for complex reactivity and stability. Three of this new type of bispidine ligands (L^1, L^2 and L^3 in Scheme 1) and their copper-dioxygen chemistry are discussed in the present report.

Results and Discussion

1. Syntheses of the Ligands and Complexes

The tetradentate ligand L^1 has been described before.[16, 25] L^1 as well as the tetradentate derivative L^2 and the dinucleating bis-tetradentate ligand L^3 are derived from the known piperidine precursor P^1 (Scheme 1);[25] formaldehyde and 4-methoxyphenylethaneamine for L^2, and *m*-xylenediamine for L^3 are the “locking groups”, which, after basic extraction with diethyl ether, produce the ligands as pure solids in reasonably good yields.

The Cu^I complexes of L^1, L^2 and L^3 were obtained from $[Cu^I(CH_3CN)_4][B(C_6F_5)_4]$ [26] and the ligands in dioxygen-free tetrahydrofurane (THF), containing several drops of acetonitrile (MeCN) to stabilize the resulting Cu^I cation; *n*-pentane was used to precipitate the complexes. It was not possible to isolate and fully characterize the Cu^IL^1 complex as a solid, even with CO used as an electron withdrawing co-ligand, which might confer extra stability. This is probably due to the aliphatic nitrogen donor set and the specific coordination geometry, which stabilize the oxidized form (the stability of the corresponding Cu^{II} complex has been determined and found to be relatively high).[16] In contrast, the yellow solid of the dinuclear complex $[Cu^I_2(L^3)][B(C_6F_5)_4)]_2$ was stable for several days, and it was also characterized in solution by ^{1}H-NMR spectroscopy. A powder of the mononuclear complex $[Cu^I(L^2)][B(C_6F_5)_4]$, obtained by addition of *n*-pentane to the reaction mixture, shows first signs of decomposition after few hours. In a CO atmosphere during the synthesis, a significantly more stable CO-substituted complex is obtained and this was used for the characterization by ^{1}H-NMR and IR spectroscopy. Cu^{II} complexes of L^2 and L^3 were obtained in good yield (60–70%) by reaction of stoichiometric amounts of the ligands and

Cu^{II} salts in MeCN (see Experimental Section), the corresponding L^1-based Cu^{II} complex has been fully characterized and the X-ray structure has been reported.[16, 25]

2. Solution Properties of the Copper Compounds

A slight broadening of the signals in the ^{1}H-NMR spectra of $[Cu^I(L^2)(CO)][B(C_6F_5)_4]$ and $[Cu^I_2(L^3)][B(C_6F_5)_4]_2$ probably results from slow oxidation of the Cu^I complexes in solution. As expected from the rigid ligand cavity and earlier structural analyses,[16, 25] no isomerism in the ligand binding mode is apparent.[21] The vibrational frequency of the carbonyl group in the IR spectrum of $[Cu^I(L^2)(CO)][B(C_6F_5)_4]$ is at 2100 cm^{-1}, *i.e.* in the expected range for *end-on* coordination of CO to Cu^I.[27, 28]

The structures of first row transition metal complexes with tetra- and pentadentate 2nd generation bispidine complexes are best described as distorted trigonal bipyramidal (tbp).[16, 25] Due to the relatively small N-Cu-N angle, enforced by the diazaheptane cycle, the Cu^{II} complexes have a "d_{x2-y2} ground state" (i.e., the unpaired electron is in d_{x2-y2}; in axial tbp symmetry the unpaired electron instead is in d_{z2}), and this is reflected in their EPR spectra.[29] That of $[Cu^{II}(L^2)(OH_2)]^{2+}$ is very similar to the spectrum of the L^1-based bispidine Cu^{II} complex (see Table 1). The electronic spectra of $[Cu^{II}(L^2)(OH_2)]^{2+}$ and $[Cu^{II}_2(L^3)(solvent)_2]^{4+}$ in MeCN have the expected *dd* transitions at approx. 600 nm; however, the low-energy transition, due to splitting of the e_g set of orbitals (in O_h) in an axial field, was not resolved for the L^2- and L^3-based complexes (Table 2).

Electrochemical measurements in MeCN indicate for $[Cu^{II}(L^2)(OH_2)]^{2+}$ an irreversible reduction at −270 mV (vs. SCE, Table 3). This potential is significantly more positive than that of $[Cu^{II}(L^1)(NCMe)]^{2+}$ (−377 mV) and suggests a higher stability of the Cu^I complex of L^2 compared to that of L^1.[29] For the dinuclear complex $[Cu^{II}_2(L^3)(solvent)_2]^{4+}$, two reduction peaks and one oxidation peak are observed (see Supporting Information for the electrochemical traces). This suggests an interaction between the two Cu^I cations in the dinuclear complex, followed by ready decomposition of the dicopper(I) complex.

3. Oxygenation Experiments

(a) Oxygenation of the copper(I) complex with L^1

Time-resolved UV-vis spectroscopy: The tetradentate ligand L^1 forms Cu^I complexes with rich oxygenation reactivity. For the oxygenation experiments, $[Cu^I(L^1)]^+$ was synthesized *in situ* [30] by addition of a $[Cu^I(MeCN)_4][B(C_6F_5)_4]$ solution in a strictly oxygen-free atmosphere to a solution of L^1 in the desired solvent and with the required concentrations. At low temperature (−80°C) in acetone, a deep blue species is generated by bubbling molecular oxygen through the *in situ* generated complex (see Figure 1); identical spectra are observed in the concentration range from $2.5\cdot10^{-4}$ M to $2\cdot10^{-3}$ M. The spectrum of the oxygenated species (see Figure 1) is dominated by a band at 618 nm with higher energy shoulders at about 520 and 450 nm. These features are in the region, where UV-vis transitions of *trans*-μ-1,2-peroxo-dicopper(II) compounds are observed, such as in the well characterized $[(Cu^{II}(Me_6tren))_2O_2]^{2+}$ [30, 31] and $[(Cu^{II}(tmpa))_2O_2]^{2+}$ [32, 33] systems. However, the intensity ratios in the L^1-based bispidine system are different to those usually observed for *end-on* peroxo-dicopper(II) complexes with local Cu^{II} trigonal bipyramidal coordination,[30, 31] and this presumably is due to the unusual coordination geometry enforced by the 2nd generation bispidine ligands (see description of the structures above). In fact, such a pattern of CT bands with "reversed intensity ratios" was shown to occur in *end-on* peroxo dicopper(II) complexes with ligands that favor local axial Cu^{II} symmetry, *i.e.*, with a d_{x2-y2} ground state.[34, 35] The *end-on* peroxo complex $[(Cu^{II}(L^1))_2O_2]^{2+}$, with 618, 520 and 450 nm absorptions appears to slowly isomerize to another, similar species, suggested to be a

conformer (see below). The isosbestic point at 420 nm indicates a clean monophasic transformation.

An intensely green solution is obtained at −120°C in 2-methyl-tetrahydrofuran (MeTHF, see Supporting Information for the spectra). In addition to the two bands at 613 and 515 nm, assigned to *trans*-$[(Cu^{II}(L^1))_2O_2]^{2+}$, there is a strong additional transition in this solvent at 452 nm, which we assign to $[Cu^{II}(L^1)O_2]^+$, *i.e.* a mononuclear η^1-superoxo-Cu^{II} complex (a similar spectrum is obtained in THF, see Supporting Information). Moreover, there is another new transition at 340 nm, which is due to a third species, probably a hydroperoxo complex ($[Cu^{II}(L^1)OOH]^{2+}$, a species with a similar spectrum is observed in diethyl ether, see Supporting Information). This putative hydroperoxo complex forms relatively slowly (see below for further characterization of this species).

Computational Analysis: DFT calculations were performed to confirm the existence of the proposed mono- and dinuclear complexes as oxygenation products of $[Cu^I(L^1)]^+$. There is a relatively large body of published computational work, especially on the theoretically challenging dinuclear systems with Cu_2O_2 "diamond" cores,[36–46] and much of this has recently been reviewed.[9] Apart from the general problem of choosing the appropriate functional,[47] the electron distribution in the "diamond" core as a function of the ligand-enforced structure clearly varies with the theoretical method used.[9, 43, 44] All spin states were considered, and the structural parameters as well as the relative stabilities are based on the widely tested and used setup involving the B3LYP functional and a triple zeta basis set (for details see Experimental Section; the energies reported include corrections for zero-point energies and solvation). The electronic transitions for the various complexes were calculated with *ab-initio* methods and time-dependent DFT (TDDFT), except for the dinuclear complex, for which, due to the larger size of the model, only a TDDFT analysis was performed. Two models were used for the computation of this complex; i) the terminal methyl groups of the three nitrogen donors (see Scheme 1) were replaced by hydrogen atoms $[(Cu^{II}(L^{1A}))_2O_2]^{2+}$; ii) the methyl groups were modeled to allow possible interactions of the methyl hydrogen atoms with the O-O bridge of $[(Cu^{II}(L^1))_2O_2]^{2+}$. The optimized structural parameters and spin densities for the lowest energy structure of the *trans*-$[(Cu^{II}(L^{1A}))_2O_2]^{2+}$ complex are listed in Table 4, together with the corresponding data for the mononuclear superoxo and the hydroperoxo complexes. All possible spin states and different orientations of the peroxo and superoxo groups (*end-on* or *side-on*) were considered and the relative energies and spin densities are given in the Supporting Information.

The dinuclear *trans*-$[(Cu^{II}(L^{1A}))_2O_2]^{2+}$ complex was modeled with three different configurations of the O-O bridge, *i.e. trans end-on* peroxo, *side-on* (μ-η^2-η^2) peroxo and bis(μ-oxo). Only the *trans*-μ-1,2-peroxo (*end-on*) structure was found to be stable; the other two collapsed on optimization to the stable isomer. Possible spin states for the *trans*-$[(Cu^{II}(L^{1A}))_2O_2]^{2+}$ complex were then considered. The open-shell singlet and triplet states are relatively close in energy (7.5 kJ/mol in favor of the singlet state). This indicates that the bis-Cu^{II} complex has a diamagnetic ground state, and antiferromagnetic coupling of the two Cu^{II} centers is also evident from their spin densities (see Table 4). Single point calculations with a larger basis and inclusion of the solvent (B2) predict the two spin states to be even closer in energy, i.e., just differing by 1.8 kJ/mol. TDDFT calculations of the dinuclear *trans*-$[(Cu^{II}(L^{1A}))_2O_2]^{2+}$ complex yield peaks of higher intensity at 580, 530 and 490 nm, and a peak with very low intensity around 670 nm; this is in acceptable agreement with the experimental absorptions at 620, 520 and 460 nm (see *e.g.* Figure 1).[48] These peaks are characteristic for charge transfer transitions. According to the DFT calculations, the absorptions at 580 nm and 530 nm correspond to the usual π^*-to-Cu CT transitions involving the peroxo group and the two Cu^{II} centers, and the lower intensity peak at 490 nm

is assigned to be due to ligand-to-metal charge transfer transitions (see Supporting Information).

As mentioned, compared to most other known *trans*-μ-peroxo dicopper complexes, the experimentally observed absorption spectrum of *trans*-$[(Cu^{II}(L^1))_2O_2]^{2+}$ is significantly different with respect to the intensities, and the TDDFT predicted transition energies are not as accurate as one might have hoped. Therefore, TDDFT calculations were also performed for the known dinuclear *trans*-μ-peroxo-Cu-tmpa complex. That absorption spectrum has a more intense peak at 530 nm and a less intense transition at 604 nm.[32, 33] The calculated spectrum of the dinuclear Cu-tmpa peroxo complex has the highest intensity peak at 567 nm, in reasonable agreement with the experimental value, within the limits of the method used. Further low intensity signals were found at 550, 530, 507 nm.

The direct reaction of O_2 with $[Cu(L^1)]^+$ results in a mononuclear superoxo-Cu^{II} complex but a mononuclear peroxo-Cu^{II} complex may also emerge from further reactions (see also experimental observations above); the peroxide and superoxide moieties can be bound in *side-on* or *end-on* orientations. The calculations predict that the superoxo complex is favored by 8.0 kJ/mol over the peroxo complex. This is mainly due to the change in the electronic configuration at the Cu^{II} center.[49] The *side-on* configuration of the superoxo complex of $[Cu^{II}(L^1)]^{2+}$ was found to be sterically hindered and reverted to the *end-on* complex on optimization. The relative energies of the triplet and open-shell singlet states of the *end-on* superoxo complex $[Cu^{II}(L^1)O_2]^+$ were found to favor the triplet state by 7.4 kJ/mol (basis set B2). The open-shell singlet state was calculated using the broken-symmetry approach that takes nondynamic correlation effects into account with DFT. TDDFT calculations of the singlet state afforded a peak at 426 nm with the maximum intensity, and this agrees well with the experimentally found range of ~410–450 nm (dependent on the solvent used, see experimental spectra). This supports the mononuclear superoxo species as a product of the oxidation of $[Cu^I(L^1)]^+$, as suggested by the low-temperature time-dependent UV-vis spectra. In fact, all of these results are in line with relatively recent findings on structurally related tetradentate tripodal ligands and corresponding η^1-superoxo-Cu^{II} species formed from their (ligand)Cu^I/O_2 reactions.[45, 52–54]; for example a triplet $S = 1$ ground state emerges from spectroscopic and computational studies[45, 53] on the X-ray structurally characterized complex $[(tmg_3tren)Cu^{II}O_2]^+$ (where tmg_3tren is 1,1,1-tris[2-[N^2-(1,1,3,3-tetramethylguanidino)]ethyl]amine).[52] Also, the prominent UV-vis spectroscopic features observed for $[Cu^{II}(L^1)O_2]^+$ are very much like those known for other established superoxo-Cu^{II}(ligand) species. [8, 45, 53–55]

Due to the relatively small size of the molecules, *ab-initio* calculations were also carried out to calculate the absorption bands of the two mononuclear complexes. The absorption spectrum of the superoxo complex $[Cu^{II}(L^1)O_2]^+$ was calculated with a reference space of (16,9), *i.e.* with two half-filled orbitals. The SORCI predicted spectrum has absorption maxima at 457 and 470 nm, in good agreement with the experimentally observed transitions. The absorption at 457 nm is a dd transition (see Figure 2). The TDDFT-calculated value of the transition for the mononuclear *end-on* hydroperoxo complex $[Cu^{II}(L^1)OOH]^+$ is in the range of ~360 nm, which is in good agreement with the experimental spectral range of 340–370 nm. SORCI calculations for this species were performed with a reference space of (19,10). The *ab-initio* calculated spectrum shows maximum intensity peaks at 336 and 415 nm and therefore supports the analysis discussed above. The major transition involved is a hydroperoxo-to-Cu^{II} LMCT transition, see Figure 2.

Resonance Raman spectra of the oxygenated copper(I) complexes with L_1: For further identification of the oxygenated $[Cu^I(L^1)]^+$ complexes, resonance Raman spectra were recorded (excitation wavelength of 623 nm, MeTHF or acetone, −80 °C; see Figure 3 and

Table 5). In MeTHF with $^{16}O_2$, two bands for the O-O stretching mode are seen at 811 cm^{-1} and 801 cm^{-1}, and these shift to one transition at 766 cm^{-1} with $^{18}O_2$. In acetone, the corresponding bands are at 816 cm^{-1} and 804 cm^{-1} with $^{16}O_2$ and at 768 cm^{-1} with $^{18}O_2$. The Cu-O vibration in MeTHF is at 547 cm^{-1} ($^{16}O_2$) and at 522 cm^{-1} ($^{18}O_2$), and the corresponding transition energies in acetone are at 550 cm^{-1} ($^{16}O_2$) and 530 cm^{-1} ($^{18}O_2$). These energies are as expected for the O-O and Cu-O modes of *trans*-μ-1,2-peroxo-Cu^{II} adducts [4] and indicate that the blue species generated in acetone at −80°C (see Figure 1) indeed is a *trans*-$[(Cu^{II}(L^1))_2O_2]^{2+}$ complex. The presence of two signals for the O-O bridge in natural abundance dioxygen might be the result of torsional isomers. DFT calculations of different torsional isomers support this assumption, and the relative energies are found to vary in a range of approx. 20 kJ/mol. The lowest energy isomer is shown in Figure 4 and has a dihedral angle of 180°, involving the $N7^a$-Cu^a-Cu^b-$N7^b$ centers. This torsional angle was varied to 0°, 30°, 60° and 90° to find the relative energies of the various conformations. The Cu-O and O-O stretching frequencies, calculated for the two lowest energy structures (180°, 120°) are presented along with the experimental values in Table 5. The O-O stretching frequencies are in reasonable agreement with the experimental frequencies, but there is some discrepancy with the Cu-O band. Another possible interpretation of the doubled peaks with the $^{16}O_2$ and one peak with the $^{18}O_2$ peroxo complex, independent of the solvent, is the occurrence of a Fermi Resonance.[45, 56–58]

EPR spectra of the oxygenated copper(I) complexes with L^1: The dinuclear *trans*-$[(Cu^{II}(L^1))_2O_2]^{2+}$ complex is antiferromagnetically coupled (see also DFT analysis above), and the mononuclear superoxo-$[Cu^{II}(L^1)O_2]^+$ species has a triplet ground state. This also emerges from the calculated spin densities of these complexes (see Table 4; there is an energy difference of 11.4 kJ/mol in favor of the triplet relative to the open-shell singlet state for the superoxo-complex $[Cu^{II}(L^1)O_2]^+$). Therefore, these complexes are not expected to show EPR transitions at liquid nitrogen temperatures,[53] and indeed, frozen solutions of the oxygenated complex in acetone and THF are EPR silent. However, a frozen solution (−80°C) of the oxygenated $[Cu^I(L^1)]^+$ complex in MeTHF, where the UV-vis spectra suggested the presence of a mononuclear hydroperoxo complex (see above), shows an EPR signal, with parameters as expected for a mononuclear hydroperoxo complex, $[Cu^{II}(L^1)(OOH)]^{2+}$ (Figure 5 and Table 6; for a dinuclear complex such as *trans*-$[(Cu^{II}(L^1))_2O_2]^{2+}$, a half-field signal would also be expected, and this was not detected here). An additional small signal of a mononuclear Cu^{II} species, also visible in Figure 5, is assigned to a minor impurity of a Cu^{II} decay product. As expected for a hydroperoxo complex, the spectrum is well resolved,[59] and, upon warming, the solution exhibits the known pattern for $[Cu^{II}(L^1)]^{2+}$.[16] The quantum-chemically computed g- and A-tensor parameters (see above and Experimental Section) are in good agreement with the experimental values for both the hydroperoxo and acetonitrile species, which was recorded and computed for comparison (see Table 6).

Reaction pathways for the oxygenation of the copper(I) complex with L^1: The L^1 based Cu^I complex has a rich oxygen activation chemistry. At least three oxygenated species are present, and the reaction pathway depends on the solvent, the relative concentrations and the temperature (see Scheme 2).

From the spectroscopic data (UV-vis, EPR, resonance Raman) and in combination with the computational characterization, we conclude that at very low temperature and in low concentrations, first an *end-on* superoxo-$[Cu^{II}(L^1)O_2]^+$ complex is formed. In acetone, diethyl ether or MeTHF at −80°C, this reacts in a very fast process to *trans*-$[(Cu^{II}(L^1))_2O_2]^{2+}$, and this is a common pathway.[4] In THF, the superoxo-$[Cu^{II}(L^1)O_2]^+$ complex is longer-lived, and it is also stabilized in MeTHF at −120°C. The dinuclear *trans*-peroxo$[(Cu^{II}(L^1))_2O_2]^{2+}$ complex (see Figure 1, acetone solution) decays slowly. In diethyl

ether and MeTHF, the *trans*-$[(Cu^{II}(L^1))_2O_2]^{2+}$ species is converted to a mononuclear hydroperoxo complex, $[Cu^{II}(L^1)(OOH)]^+$, which also can be prepared from $[Cu^{II}(L^1)]^{2+}$ and H_2O_2. Reaction mixtures studied were warmed to ambient temperature, and from those solutions electrospray ionization mass spectra (ESI-MS) were recorded, which reveal $[Cu^{II}(L^1)]^{2+}$ as the main decomposition fragment, and only traces of species with an oxygenated ligand backbone.

(b) Oxygenation of the copper(I) complex with L^2—L^2 has a ligand cavity which is identical to that of L^1 but the ligand has a methoxy-substituted phenyl ring (see Scheme 1) in order to potentially mimic an enzymatic substrate found in close proximity to the Cu^I/O_2 derived site. In spite of the seemingly small change in ligand structure compared to L^1, the Cu^I-dioxygen chemistry is very different. In view of the observed redox potentials, this is not entirely unexpected (see above and Table 3). As oxygenation product, only one intensely green species with maxima in the electronic spectra at ca. 400 and 650 nm was found, independent of the solvent (acetone, THF, MeTHF), temperature (−80°C to −120°C) and concentration ($c = 2\cdot10^{-4}$ M to $2.5\cdot10^{-3}$ M; see Figure 6).

The UV-vis spectrum is as expected for a mononuclear η^1-superoxo-$[Cu^{II}(L^2)O_2]^+$ complex,[4, 30] see also above. The clean isosbestic point suggests that this is the only oxygenation product. This is also supported by the fact that the relative intensities of the two bands at 664 and 402 nm do not change (2.1–2.4 (402 nm) to 1 (664 nm)) if the concentration is varied over the range $c = 2\cdot10^{-4}$ M to $2.5\cdot10^{-3}$ M.

The Cu^{II}-superoxo oxygenation product is stable at −80 °C for about 24 h. If warmed to room temperature, the color changes from intensely green to very light green. On cooling again to −80°C, the dark green color is reproduced, *i.e*. binding of dioxygen and formation of the mononuclear superoxo complex (temperature-dependent equilibrium) is to a large extent reversible (see Figure 7), and this behavior appears to be the first such example thus far reported. The amount of dioxygen liberated on warming of the reaction mixture was determined quantitatively with pyrogallol as indicator (see Experimental Section):[60] in a solution of $1.0\cdot10^{-3}$ mol/l of $[Cu^I(L^2)]^+$ (THF, −80°C), the reversibly bound dioxygen is determined to be 75% of the expected amount (see Supporting Information). The decomposition of the L^2-based superoxo complex $[Cu^{II}(L^2)O_2]^+$ was also followed spectrophotometrically (THF, −35°C), and the resulting half-life time is $t_{1/2} = 30$ min. Figure 8 shows a first-order decay kinetic trace, and this emphasizes the existence of only one oxygenation product (*i.e*. the superoxo complex), which decomposes to $[Cu^{II}(L^2)]^{2+}$. This is further supported by ESI mass spectrometry, where $[Cu^{II}(L^2)]^{2+}$ was detected as the main decomposition product.

DFT calculations on the superoxo complex $[Cu^{II}(L^2)O_2]^+$ were performed and found that the triplet state with an *end-on* orientation is 11.9 kJ/mol lower in energy than the *side-on* oriented singlet state.

(c) Comparison of the two systems based on ligands L^1 and L^2—Although the structural difference between the ligands L^1 and L^2 is small, the copper-dioxygen chemistry is very different. Therefore, the O_2 binding energies between the two systems and the steric hindrance induced by the aromatic moiety on formation of the dinuclear L^2-based complex were studied by DFT calculations. The optimized structure of the mononuclear superoxo complexes $[Cu^{II}(L^1)O_2]^+$ and $[Cu^{II}(L^2)O_2]^+$, and of the corresponding dinuclear *trans*-peroxo complexes, together with relevant structural parameters, are shown in Figure 9. Similar to the mononuclear L^1-based superoxo complex, the triplet and the open shell singlet species are relatively close in energy for the L^2-based system. The strain accompanying the formation of the dinuclear *trans*-peroxo-$[(Cu^{II}(L^1))_2O_2]^{2+}$ complex was calculated by

modification of the optimized $[(Cu^{II}(L^2))_2O_2]^{2+}$ complex to yield the corresponding L^1-based dicopper(II) species, followed by a single point calculation. The resulting approximate strain energy for the formation of the dinuclear peroxo-complex $[(Cu^{II}(L^2))_2O_2]^{2+}$, induced by the N7-based substituent in L^2 is 79.8 kJ/mol. A considerable strain also emerges from the optimized geometry of the dinuclear L^2- in comparison to the L^1-based complex shown in Figure 9: the slightly elongated Cu-O distances (0.02–0.04 Å) for the L^2-based complex compared to that of the L^1-based system, reveal the steric hindrance that may prevent the ready formation of the dinuclear complex. In addition, the binding of superoxide and peroxide to mono- and dinuclear $Cu^{II}(L^1)$ and $Cu^{II}(L^2)$ complexes was compared: in the mononuclear case, formation of the *end-on*-superoxo-$[Cu^{II}(L^1)O_2]^+$ complex is favored over the $[Cu^{II}(L^2)O_2]^+$ analogue by 11.1 kJ/mol. Similarly, the peroxo binding energy for the dinuclear species is found to be in favor of the L^1-based complex by 20.3 kJ/mol. Both findings are largely due to the sterics of the methoxy phenylethyl group and are in agreement with the experimental observations.

(d) Oxygenation of the dicopper(I) complex with L^3—The ligand L^3 with its *meta*-xylene bridge provides the possibility to form both *trans*-peroxo complexes (Cu : O_2 ratio of 2 : 1) and complexes which are oxygenated at both copper centers (Cu : O_2 ratio of 2 : 2). The electronic spectrum generated at −80°C in acetone ($c = 1.3 \cdot 10^{-3}$ M) has two bands at 334 nm and 406 nm, as well as a weak band at 637 nm (see Supporting Information). The oxygenation product is not stable, *i.e.* the band at 406 nm decays within 60 min at −80°C. The assignment of the spectra to specific oxygenated complexes is not unambiguous.

The UV-vis spectrum of oxygenated $[Cu^I_2(L^3)]^{2+}$ at −120°C in MeTHF has three bands at 412 nm, 563 nm and 678 nm (see Supporting Information). These electronic transitions are typical for an *end-on* superoxo complex.[55] Although the structure of $[Cu^I_2(L^3)]^{2+}$ allows for both *trans*-peroxo and *end-on* superoxo, the *end-on* superoxo complex seems to be preferred due to the steric strain induced by a potential *trans*-peroxo bridge. After warming to −80°C the three bands decrease in intensity, and a new band at 398 nm is formed. This is very similar to the spectrum observed in acetone. A solution of the oxygenated complex (−120°C) was allowed to warm up to ambient temperature and was then analyzed by ESI mass spectrometry. Interestingly, a partially oxidized ligand was characterized (see Supporting Information). The main fragment is a bispidine-derived aldehyde, which is proposed to be formed by attack at the CH-benzylic position near to the *meta*-xylene group (see Scheme 3, see also Supporting Information). This is not an unexpected reaction, and similar pathways have been described before.[55, 61–63] However, at this time we cannot be sure about what species is effecting the oxidative N-dealkylation reaction, a superoxo, $(Cu^{II})_2$-peroxo or another $[Cu^I_2(L^3)]^{2+}/O_2$ derived species.

Conclusions

The Cu^I complexes of three 2nd generation bispidine ligands (one of them dinucleating) were oxygenated, and the oxygenation products as well as their formation and decay pathways were studied. Due to the high reactivity of the copper(I) precursors and the intermediates, the characterization of some of the species involved is not unambiguous if taken alone. However, the thorough spectroscopic analysis of some key species as well as their computational analysis leads to a self-consistent overall picture of the systems.

The μ-peroxo-dicopper(II) complex of the L^1-based ligand is thoroughly characterized by its time-dependent UV-vis spectra and the resonance Raman transitions with $^{16}O_2$ and $^{18}O_2$ labeled peroxo brides. The computational analysis in this case leads to a better understanding of a few details but primarily serves to validate the theoretical model used. Also well characterized is the mononuclear hydroperoxo-copper(II) complex of L^1, and this

is primarily based on the EPR spectrum, which is compared to other copper(II)-L^1 spectra and, importantly, in good agreement with the computed spectrum. The time-dependent UV-vis spectra support these assignments and show the various pathways for interconversion between the various species. The third species which can be assigned without much speculation is the mononuclear superoxo-copper(II) complex of L^2. The assignment primarily is based on the clean formation equilibrium which only involves two copper-based species, the copper(I) complex of L^2 and the corresponding superoxo-copper(II) complex. This is a clean 1 : 1 (Cu^I : O_2) reaction, and we have shown that it is reversible over many cycles (with a minor amount of decay products formed, as one would expect), and the superoxo-copper(II) complex has the expected electronic properties; specifically its UV-vis spectrum has the expected transitions. Based on this assignment of the L^2-based superoxo-copper(II) complex, we are able to also assign the much more reactive L^1-based superoxo-copper(II) complex due to its time-dependent UV-vis spectrum because the two structures are very similar to each other (as expected, and supported by the DFT-optimized structures), and the assignment of the L^1-based superoxo complex is also strongly supported by the computed UV-vis spectra. We therefore believe that all important species in the L^1- and L^2-based complexes are part of a self-consistent interpretation with well characterized key species. The compounds involved in the L^3-based copper-dioxygen chemistry are not well characterized, and this system is only presented here to show possible pathways and reactivities of these systems. Of specific interest is the very different stabilities/reactivities of the L^1- and L^2-based superoxo-copper(II) complexes, and it is quite clear that this is a result of efficient shielding of the active site with the L^2 ligand substituent. Small geometric differences, as observed in L^3, which leads to amine dealkylation supports this interpretation and points toward future studies of the reactivities of these superoxo complexes with external substrates.

It is of interest to compare the systems presented here with those based on other ligand systems. The main difference between 1st and 2nd generation bispidine ligands is in terms of the structures they enforce to the metal ions – clearly, the difference in donor sets also is of importance, specifically with respect to the redox potentials, which obviously are of importance in terms of oxygen activation: while the 1st generation bispidines enforce square pyramidal geometries with very stable μ-peroxo-dicopper(II) (in-plane-coordinated peroxo group), the 2nd generation bispidines lead to distorted trigonal bipyramidal complexes with an apical peroxo group – note that the ligand-enforced distortion from trigonal symmetry leads to a d_{x2-y2} ground state and to a reactivity which not only strongly differs from that of the 1st generation bispidine-based systems but also from those of other ligands discussed in the literature.

Experimental Section

Materials and measurements

Chemicals (Aldrich, Fluka) were used without further purification if not otherwise stated. L^1 and $[Cu^{II}(L^1)(NCCH_3)](BF_4)_2$ were described before.[25] *NMR spectra* were recorded at 200.13 MHz (^1H) and 50.33 MHz (^{13}C) on a Bruker AS-200 or a Bruker DRX-200 instrument with the solvent signals used as reference. *IR spectra* were recorded with a Perkin Elmer Spectrum 100 FT-IR spectrometer instrument from KBr pellets. *Mass spectra* were obtained with a JEOL JMS-700 or Finnigan TSQ 700/Bruker ApexQe hybrid 9.4 FT-ICR instrument. *Electronic spectra* were measured with a Tidas II J&M or a Jasco V-570 UV/Vis/NIR-spectrophotometer. *EPR measurements* were preformed on a Bruker ELEXSYS-E-500 instrument at 125 K; spin-Hamiltonian parameters were obtained by simulation of the spectra with XSophe.[64] For *electrochemical measurements* a BAS-100B workstation was used, with a three-electrode setup, consisting of a glassy carbon working, a Pt-wire auxiliary and, for MeCN solutions, an $Ag/AgNO_3$ reference electrode (0.01M

$AgNO_3$, 0.1M $(Bu_4N)(PF_6)$, degassed CH_3CN), solutions of the complexes in MeCN/0.1M $(Bu_4N)(PF_6)$; the potential of the Fc^+/Fc-couple for the MeCN setup had a value of +91 mV (MeCN, scan rate of 100mV/s). Elemental analyses were obtained from the analytical laboratories of the chemical institutes at the University of Heidelberg on a Vario EL (Elementary) instrument.

Computational details

The presence of various oxygenated species on reaction with each of the three bispidine ligands was supported by theoretical calculations. Geometry optimizations and frequency calculations were carried out using Jaguar[65] employing the hybrid density functional, B3LYP[66, 67] and the effective core pseudopotential, LACVP (basis B1).[68] The effect of solvent and a larger basis set, LACV3P**++ (designated as B2) were used for single point calculations on the LACVP optimized geometries. Acetonitrile was used as the solvent with an epsilon of 37.5 and a probe radius of 2.183 as implemented in Jaguar. Initially, the non-hybrid functional BP86 was used to calculate the relative energies of various orientations of the copper-dioxygen complexes. However, side-on orientation of the mononuclear $[Cu^I(L^1)O_2]^{2+}$ complex failed to optimize at the BP86 method. With B3LYP there were no such problems, and this functional is widely used for the study of reaction mechanisms of copper-dioxygen complexes.[69] Spectroscopic calculations were carried out using the program ORCA.[70, 71] TDDFT calculations were performed using the B3LYP functional and a triple-zeta basis set, TZVP[72] on Cu and all heavy atoms, with the split-valence basis for the rest of the molecule (SV(P)). Due to the computational expense, the effect of solvent was not considered in the TDDFT calculations. EPR calculations involved the BHLYP[73] functional and the CP(PPP) basis[74] on the metal, the IGLO-III[75] basis set on the atoms directly bound to Cu and the SV(P), SV/J basis for the rest of the atoms. Multi reference-configuration interaction (MRCI) calculations for prediction of absorption spectra were carried out using the spectroscopy-oriented CI (SORCI) method.[70] Appropriate reference spaces were chosen for the complexes.[44] The initial orbitals for these calculations were chosen from a BP86[76, 77] calculation which produced quasi-restricted orbitals and were rotated to form an adequate active space. The thresholds T_{sel}, T_{pre} and T_{nat} for these MRCI calculations were set to 10^{-6}, 10^{-5} and 10^{-5} respectively, and were shown to enhance the computational efficiency with a minimal loss of accuracy.[70] Resonance Raman spectra were calculated on BP86/TZVP optimized geometries and checked for zero imaginary frequencies with the same method. The vibrational frequencies were not scaled for the complexes discussed here. If not mentioned otherwise, the relative energies reported in the paper include zero-point corrections and solvent effects.

Low temperature oxygenation experiments—The in situ generated Cu^I complexes were prepared in the appropriate solvent using $Cu^I(CH_3CN)_4(B(C_6F_5)_4$,[26] to which was added a solution of an equimolar amount of the appropriate ligand. After standing for 5–10min, the reaction solution was cooled (about 15 min) and molecular oxygen was bubbled through the solution for 5–15 s. THF, MeTHF and diethyl ether (without stabilizers) were used for −80°C measurements (cold bath: acetone, dry ice, controlled by a thermometer). For the measurements at −120°C (cold bath = liquid nitrogen, *n*-pentane, temperature controlled by thermometer) MeTHF was used as solvent.

Quantitative measurement of molecular oxygen concentrations—Five reaction flasks were charged with 0.4 g pyrogallol each and dissolved in 10 ml of deoxygenated NaOH (33% in H_2O) each in a glovebox. After removing them from the glovebox 0.2, 0.4, 0.6, 0.8 and 1.0 ml of dioxygen were added via gastight syringe and the flasks were reintroduced into the glovebox. After 18 hours, 0.2 ml of the total volume was transferred to a crown-capped quartz–cuvette and diluted with 1.8 ml of deoxygenated NaOH (33% in

H_2O). From the calibration and using linear regression results, y = 1.5885x − 0.0558, R2 = 0.9952 with NaOH (33% in H_2O) as baseline. The samples were then treated similarly. The flask with the pyrogallol solution was connected to the warmed-up reaction solution this was closed using a piece of plastic tubing, before opening the sample flask to the flask with pyrogallol solution. The reaction solution was left stirring for 18 h, until 0.2 ml of the flask with pyrogallol had been introduced in a capped cuvette diluted with 1.8 ml of deoxygenated NaOH (33% in H_2O) and analyzed.

$[Cu^{II}(L^1)(OOH)]^{2+}$—$[Cu^{II}(L^1)(NCCH_3)](BF_4)_2$ (4 mg) was dissolved in 10 ml of MeOH to give a $5.5{\cdot}10^{-4}$ mol/l solution This was cooled to −80°C, and 0.1 ml NEt_3 and 0.2 ml of H_2O_2 (30% wt in water) were slowly added. The initially blue reaction solution instantly turned to violet. This color faded away when the solution was left to warm to room temperature. At −80°C the violet species was stable for at least 0.5 h enabling physical measurements to be applied.

Syntheses—*Caution:* Although no difficulties were found using the perchlorate salts described, these are potentially explosive and need to be handled with care. Heating, especially when dry, must be avoided.

L^2. 3-(4-methoxyphenethyl)-1,5-diphenyl-7-(1,4,6-trimethyl-1,4-diazepan-6-yl)-3,7-diazabicyclo [3.3.1]nonan-9-one—1.53 mmol of 4-methoxyphenylethanamine, 3.06 mmol formaldehyde solution and 0.35 ml glacial acetic acid were mixed at 0°C in 4 ml MeOH. The ice bath was removed and 1.53 mmol of 1-(1,4,6-Trimethyl-1,4-diazacycloheptane-6-yl)-3,5- diphenylpiperidine-4-one in 2 ml MeOH were added. The reaction mixture was stirred for 8 h at 65°C. The solvent was removed in vacuo. The resulting oily solid was dissolved in dichloromethane and the pH was adjusted using KOH to about pH ~13 and this solution was extracted with 30 ml dichloromethane three times. The combined organic phases were dried with Na_2SO_4. The solvent was removed to yield a white solid (1.00 mmol, 67%.).*^{1}H-NMR* ($CDCl_3$, 200.13 MHz) δ = 1.12 (s, 3H, C-CH_3); 2.21 (s, 6H, N-CH_3); 2.23 (d, ^{2}J = 13.8 Hz, 2H, C-CH_{2ax}); 2.45 (m, 4H, CH_2-CH_2); 2.75 (d, ^{2}J= 13.8 Hz, 2H, C-CH_{2eq}); 2.78 (m, 4H, N-CH_2-CH_2-PhOMe); 3.07 (d, ^{2}J = 10.6 Hz, 2H, CH_{2ax}-N-CH_2-CH_2); 3.25 (d, ^{2}J= 11.0 Hz, 2H, N-CH_{2ax}-C); 3.51 (d, ^{2}J= 10.6 Hz, 2H, CH_{2eq}-N-CH_2-CH_2); 3.72 (d, ^{2}J= 11.0 Hz, 2H, N-CH_{2eq}-C); 3.75 (s, 3H, O-CH_3); 7.14 (d, ^{3}J= 8.8 Hz, 2H, CH_{ar}-C-O-CH_3); 7.26 (m, 12H, CH_{Ph}) ppm. *^{13}C-NMR* ($CDCl_3$, 50.27 MHz) 25.10 (1C, C-CH_3); 32.95 (1C, CH_2-PhOMe); 48.80 (2C, N-CH_3); 54.60 (1C, C-CH_3); 55.23 (1C, O-CH_3); 58.67 (1C, CH_2-CH_2-PhOMe); 59.41 (2C, CH_2-CH_2), 60.12 (2C, C-C_{Ph}); 62.11 (2C,N-CH_2-C-C_{Ph}); 64.60 (2C, N-CH_2-C-CH_3); 66.16 (2C, CH_2-N-CH_2-CH_2); 113.80 (1C, $C_{MeO/o}$); 126.43 (2C, $C_{Ph/p}$); 126.85 (4C, $C_{Ph/m}$); 127.83 (4C, $C_{Ph/o}$); 129.53 (2C, $C_{MeO/o}$); 132.20 (1C, CH_2-C_{MeO}); 143.62 (2C, O-C_{MeO}); 157.92 (1C, C_{Ph}); 211.70 (1C, CO) ppm. *IR (KBr-pellet)* 3026; 2935; 2802; 1731; 1611; 1512; 1462; 1447; 1246; 758; 715, 698 cm^{-1}. ESI *MS (MeOH) m/z* 599.21 $[L^2H(CH_3OH)]^+$, 567.21 $[L^2H]^+$. *Elemental analyses (L2x0.5H_2O)* calc.: C: 75.10, H: 8.23, N: 9.73 found: C: 75.18, H: 8.34, N: 9.50.

L^3. (7,7′-(1,3-phenylenebis(methylene))bis(1,5-diphenyl-3-(1,4,6-trimethyl-1,4-diazepan-6-yl)-3,7- diazabicyclo[3.3.1]nonan-9-one))—0.18 ml (1.36 mmol) *m*-xylylendiamine, 1.1g P^1 (2.8 mmol) and a H_2CO solution (37%) 0.46 ml (6.2 mmol) were dissolved in 10 ml THF, 10 ml DME, 6 ml HOAc. The reaction mixture was stirred at 80°C for 18h where upon the solvent was removed in vacuo. The resulting oily solid was suspended in 2M HCl and this aqueous phase extracted once using diethyl ether. Using KOH, the pH was adjusted to pH~13 and the resulting solution extracted three times with 30 ml dichloromethane. The combined organic phases were dried with Na_2SO_4 and the solvent

removed to yield 800 mg (0.83 mmol) of product, 61%. NMR: *^{1}H-NMR* ($CDCl_3$, 200.13 MHz) δ = 1.22 (s, 6H, C-CH_3), 2.32 (m, 16H, N-CH_3, C-CH_{2ax}-N); 2.53 (m, 8H, CH_2-CH_2); 2.88 (d, ^{2}J= Hz, 4H, C-CH_{2eq}-N); 3.15 (d ^{2}J= 10.6Hz, 4H, CH_{2ax}-N-CH_2-Py); 3.33 (d, 4H, CH_{2ax}-N-C-CH_3); 3.56 (d ^{2}J= 10.6Hz, 4H, CH_{2eq}-N-CH_2-Xyl); 3.75 (s, 4H, CH_2-Xyl); 3.89 (d, 4H, CH_{2eq}-N-C-CH_3), 53(s, 4H, CH_2-Xyl); 3.70(s, 4H, CH_2-Xyl); 7.10–7.24 (m, 20H, CH_{Ph}) ppm. ESI Mass: m/z 967.63 (100%)$(L^3H)^+$. *IR (KBr-pellet)*: 3650; 3385; 3025; 2939; 2805; 1728; 1601; 1446; 1348; 1286; 1135; 1039; 918; 751; 716; 698 cm^{-1}. *Elemental analyses (L^3xH_2O)* calc.: C: 75.57, H: 8.18, N: 11.37 found: C: 75.64, H: 8.11, N: 11.55.

$[Cu^{II}(L^2)](ClO_4)_2$—0.09 mmol $Cu^{II}(ClO_4)_2(H_2O)_6$ were dissolved in 2 ml CH_3CN and added to solution of 0.09 mmol L^2 in 2 ml CH_3CN. After stirring at ambient temperature overnight, the resulting blue solution was treated with a diethyl ether diffusion resulting in a green solid 65% yield (0.06 mmol). *IR (KBr-pellet)*: 3548; 3016; 2974; 2839; 1740; 1660; 1611; 1514; 1448; 1250; 1098; 700; 624 cm^{-1}. *($E_{1/2}$, CH_3CN, 100 mV/s):* -270_{irr} mV *ESI$^+$MS (MeOH) m/z* 728.08 $[Cu^{II}(L^2)(ClO4)]^+$, 674.14 $[Cu^{II}(L^2)(HCOO)]^+$, 629.30 $[Cu^{II}(L^2)]^+$. *Elemental analyses ($[Cu^{II}(L^2)](ClO_4)_2 \cdot 3.5\ H_2O$)* calc.: C: 48.51, H: 5.88, N: 6.29 found: C: 48.42, H: 5.81, N: 6.46. An X-ray structure of this complex was obtained, and it has the expected coordination geometry;[16, 25] however the quality of the structure (R ~ 9%) precludes its publication.

$[Cu_2^{II}(L^3)](BF_4)_4$—0.80 mmol $Cu^{II}(BF_4)_2$ $(H_2O)_6$ were dissolved in 3 ml CH_3CN and added to solution of 0.41 mmol L^3 in 3 ml CH_3CN. After stirring at RT overnight, the resulting green-blue solution was treated with a diethyl ether diffusion resulting in a blue solid 73% yield (0.30 mmol). Precipitation of the product could also be carried using MeOH as solvent along with a diethyl ether diffusion. *IR (KBr-pellet)*: 3619; 3555; 3030; 2953; 2876; 1743; 1693; 1603; 1500; 1448; 1367; 1320; 1283; 1059; 764; 699 cm^{-1}. *($E_{1/2}$, CH_3CN, 100 mV/s):* -396_{ox} mV, -697_{ox} mV, -555_{red} mV, *ESI$^+$MS (MeCN) m/z* 592.18 $[Cu^{II}_2(L^3)](OH)(F)(H_2O)_2^{2+}$. *Elemental analysis* ($[Cu_2^{II}(L^3)](BF_4)_2(F)_2 \times 2$ MeOH) calcd.: C: 56.40, H: 6.41, N: 8.10 found: C: 56.52, H: 6.04, N: 7.86.

$[Cu^I(L^3)](B(C_6F_5)_4)$—0.21 mmol $Cu^I(B(C_6F_5)_4(CH_3CN)_4$ and 0.10 mmol L^3 were stirred in 5 ml rigorously deoxygenated THF with 3 drops of CH_3CN under an oxygen free atmosphere. After 30 min of stirring, 50 ml deoxygenated n-pentane was added to precipitate the product. The solid was collected and the solvent removed in vacuo to yield 73 % yield (0.07 mmol) as a yellow powder.

Supplementary Material

Refer to Web version on PubMed Central for supplementary material.

Acknowledgments

Generous financial support by the German Science Foundation (DFG) and the University of Heidelberg (LGFG, “Molecular probes”) is gratefully acknowledged. K. D. K. acknowledges financial support from the National Institutes of Health of the USA.

References

1. Que L Jr, Tolman WB. Angew Chem Int Ed. 2002; 41:1114.
2. Holland PL, Tolman WB. Coord Chem Rev. 1999; 192:855.
3. Kaim W, Rall J. Angew Chem Int Ed. 1996; 35:43.
4. Mirica LM, Ottenwaelder X, Stack TDP. Chem Rev. 2004; 104:1013. [PubMed: 14871148]

5. Karlin KD, Kaderli S, Zuberbühler AD. Acc Chem Res. 1997; 30:139.
6. Schindler S. Eur J Inorg Chem. 2000; 719
7. Hatcher LQ, Karlin KD. J Biol Inorg Chem. 2004; 9:669. [PubMed: 15311336]
8. Itoh S. Curr Opin Chem Biol. 2006; 10:115. [PubMed: 16504568]
9. Gherman BF, Cramer CJ. Coord Chem Rev. 2009; 253:723.
10. Kitajima N, Moro-oka Y. Chem Rev. 1994; 94:737.
11. Solomon EI, Tuczek F, Root DE, Brown CA. Chem Rev. 1994; 94:827.
12. Itoh, S. Copper-Oxygen Chemistry. Karlin, KD.; Itoh, S., editors. Wiley & Sons; Weinheim, New York: 2011. p. 225
13. Mannich C, Mohs P. Chem Ber. 1930; B63:608.
14. Comba P, Nuber B, Ramlow A. J Chem Soc, Dalton Trans. 1997; 347
15. Comba P, Kerscher M, Schiek W. Prog Inorg Chem. 2007; 55:613.
16. Comba P, Haaf C, Wadepohl H. Inorg Chem. 2009; 48:6604. [PubMed: 19456149]
17. Börzel H, Comba P, Katsichtis C, Kiefer W, Lienke A, Nagel V, Pritzkow H. Chem Eur J. 1999; 5:1716.
18. Börzel H, Comba P, Hagen KS, Katsichtis C, Pritzkow H. Chem Eur J. 2000; 6:914. [PubMed: 10826614]
19. Börzel H, Comba P, Pritzkow H. J Chem Soc, Chem Commun. 2001; 97
20. Comba P, Lienke A. Inorg Chem. 2001; 40:5206. [PubMed: 11559083]
21. Börzel H, Comba P, Hagen KS, Kerscher M, Pritzkow H, Schatz M, Schindler S, Walter O. Inorg Chem. 2002; 41:5440. [PubMed: 12377039]
22. Comba P, Merz M, Pritzkow H. Eur J Inorg Chem. 2003; 1711
23. Born K, Comba P, Daubinet A, Fuchs A, Wadepohl H. J Biol Inorg Chem. 2007; 12:36. [PubMed: 16964505]
24. Comba P, Martin B, Muruganantham A, Straub J. in preparation.
25. Comba P, Haaf C, Lienke A, Muruganantham A, Wadepohl H. Chem Eur J. 2009; 15:10880. [PubMed: 19746459]
26. Liang H-C, Kim E, Incarvito CD, Rheingold AL, Karlin KD. Inorg Chem. 2002; 41:2209. [PubMed: 11952376]
27. Karlin KD, Cruse RW, Gultneh Y, Farooq A, Hayes JC. J Am Chem Soc. 1987; 109:2668.
28. Rondelez Y, Séneque O, Rager M-N, Duprat AF, Reinaud O. Chem Eur J. 2000; 6:4218. [PubMed: 11128287]
29. Note that the coligand (H_2O, MeCN, MeOH or a counterion, according to the elemental analyses, see experimental section), is expected to exchange in solution, i.e. for the spectra and CV in Tables 1 – 3 and discussed in the text, these are assumed to be identical and correspond to the solvent.
30. Becker M, Heinemann FW, Schindler S. Chem Eur J. 1999; 5:3124.
31. Weitzer M, Schindler S, Brehm G, Schneider S, Hoermann E, Jung B, Kaderli S, Zuberbueheler AD. Inorg Chem. 2003; 42:1800. [PubMed: 12639112]
32. Jacobson RR, Tyeklar Z, Farooq A, Karlin KD, Liu S, Zubieta J. J Am Chem Soc. 1988; 110:3690.
33. Baldwin MJ, Ross PK, Pate JE, Tyeklar Z, Karlin KD, Solomon EI. J Am Chem Soc. 1991; 113:8671.
34. Lee D-H, Hatcher LQ, Vance MA, Sarangi R, Milligan AE, Sarjeant AAN, Incarvito CD, Rheingold AL, Hodgson KO, Hedman B, Solomon EI, Karlin KD. Inorg Chem. 2007; 46:6056. [PubMed: 17580938]
35. Lee Y, Lee D-H, Park GY, Lucas HR, Sarjeant AAN, Kieber-Emmons MT, Vance MA, Milligan AE, Solomon EI, Karlin KD. Inorg Chem. 2010; 49:8873. [PubMed: 20822156]
36. Cramer CJ, Pak Y. Theor Chem Acc. 2001; 105:477.
37. Cramer CJ, Kinsinger CK, Pak Y. J Mol Struct, Theor Chem. 2003; 632:111.
38. Spuhler P, Holthausen MC. Angew Chem. 2003; 42:5961. [PubMed: 14679543]
39. Mirica LM, Vance M, Rudd DJ, Hedman B, Hodgson KO, Solomon EI, Stack TDP. Science. 2005; 308:1890. [PubMed: 15976297]

40. Lind T, Siegbahn PEM, Crabtree RH. J Phys Chem B. 1999; 103:1193.
41. Siegbahn PEM, Wirstam M. J Am Chem Soc. 2001; 123:11819. [PubMed: 11716748]
42. Siegbahn PEM. J Biol Inorg Chem. 2003; 8:577. [PubMed: 12764603]
43. Cramer CJ, Wloch M, Piecuch P, Puzzarini C, Gagliardi L. J Phys Chem A. 2006; 110:1991. [PubMed: 16451035]
44. Huber SM, Shahi ARM, Aquilante F, Cramer CJ, Gagliardi L. J Chem Theory Comput. 2009; 5:2967.
45. Woertink JS, Tian L, Maiti D, Lucas HR, Himes RA, Karlin KD, Neese F, Würtele C, Holthausen MC, Bill E, Sundermeyer J, Schindler S, Solomon EI. Inorg Chem. 2010; 49:9450. [PubMed: 20857998]
46. Maiti D, Lee DH, Gaoutchenova K, Würtele C, Holthausen MC, Sarjeant AAN, Sundermeyer J, Schindler S, Karlin KD. Angew Chem Int Ed. 2008; 47:82.
47. Atanasov M, Comba P, Martin B, Müller V, Rajaraman G, Rohwer H, Wunderlich S. J Comp Chem. 2006; 27:1263. [PubMed: 16786541]
48. Note that the transition energies are dependent on the solvent, and solvation has not been considered in our TDDFT calculations.
49. Note that single determinantal methods such as DFT do not allow to compute the wavefunction of the superoxo complex in a single optimization.[50, 51]
50. Pantazis DA, McGrady JE. Inorg Chem. 2003; 42:7734. [PubMed: 14632488]
51. Benjamin F, Gherman BF, Cramer CJ. Inorg Chem. 2004; 43:7281. [PubMed: 15530076]
52. Würtele C, Gaoutchenova E, Harms K, Holthausen MC, Sundermeyer J, Schindler S. Angew Chem, Int Ed. 2006; 45:3867.
53. Lanci MP, Smirnov VV, Cramer CJ, Gauchenova EV, Sundermeyer J, Roth JP. J Am Chem Soc. 2007; 129:14697. [PubMed: 17960903]
54. Maiti D, Fry HC, Woertink JS, Vance MA, Solomon EI, Karlin KD. J Am Chem Soc. 2007; 129:264. [PubMed: 17212392]
55. Kunishita A, Kubo M, Sugimoto H, Ogura T, Sato K, Takui T, Itoh S. J Am Chem Soc. 2009; 131:2788. [PubMed: 19209864]
56. Henson MJ, Vance MA, Zhang CX, Liang H-C, Karlin KD, Solomon EI. J Am Chem Soc. 2003; 125:5186. [PubMed: 12708870]
57. Lee Y, Park GY, Lucas HR, Vajda PL, Kamaraj K, Vance MA, Milligan AE, Woertink JS, Siegler MA, Narducci Sarjeant AA, Zakharov LN, Rheingold AL, Solomon EI, Karlin KD. Inorg Chem. 2009; 48:11297. [PubMed: 19886646]
58. Peterson RL, Himes RA, Kotani H, Suenobu T, Tian L, Siegler MA, Solomon EI, Fukuzumi S, Karlin KD. J Am Chem Soc. 2011; 133:1702.
59. Kodera M, Kita T, Miura I, Nakayama N, Kawata T, Kano K, Hirota S. J Am Chem Soc. 2001; 123:7715. [PubMed: 11481001]
60. Ghiladi RA, Huang H-W, Moënne-Loccoz P, Stasser J, Blackburn NJ, Woods AS, Cotter RJ, Incarnato CD, Rheingold AL, Karlin KD. J Biol Inorg Chem. 2005; 10:63. [PubMed: 15583964]
61. Shearer J, Zhang CX, Zakharov LN, Rheingold AL, Karlin KD. J Am Chem Soc. 2005; 127:5469. [PubMed: 15826184]
62. Maiti D, Narducci Sarjeant AA, Karlin KD. J Am Chem Soc. 2007; 129:6720. [PubMed: 17474748]
63. Sanyal I, Mahroof-Tahir M, Nasir S, Ghosh P, Cohen BI, Gultneh Y, Cruse R, Farooq A, Karlin KD, Liu S, Zubieta J. Inorg Chem. 1992; 31:4322.
64. Wang D, Hanson GR. Appl Magn Reson. 1996; 11:401.
65. Schrödinger. JAGUAR 5.5, 6.5, Jaguar 5.5, Jaguar 6.5. Schrödinger LLC; New York, NY: 2005.
66. Becke AD. J Chem Phys B. 1993; 98:5648.
67. Lee C, Yang W, Parr RG. Phys Rev B. 1988; 37:785.
68. Hay PJ, Wadt WR. J Chem Phys. 1985; 82:270.
69. Güll M, Luis JM, Sola M, Siegbahn PEM. J Biol Inorg Chem. 2009; 14:229. [PubMed: 18972140]
70. Neese F. J Chem Phys. 2003; 119:9428.

71. Neese F. Int J Quant Chem. 2001; 83:104.
72. Schäfer A, Huber C, Ahlrichs R. J Chem Phys. 1994; 100:5829.
73. Holthausen MC, Heinemann C, Cornehel HH, Koch W, Schwarz H. J Chem Phys. 1995; 102:4931.
74. Neese F. Inorg Chim Acta. 2002; 337C:181.
75. Kutzelnigg, W.; Fleischer, U.; Schindler, M. NMR-Basic Principles and Progress. Springer; Heidelberg: 1990.
76. Becke AD. Phys Rev A. 1988; 38:3098. [PubMed: 9900728]
77. Perdew JP. Phys Rev B. 1986; 33:8822.

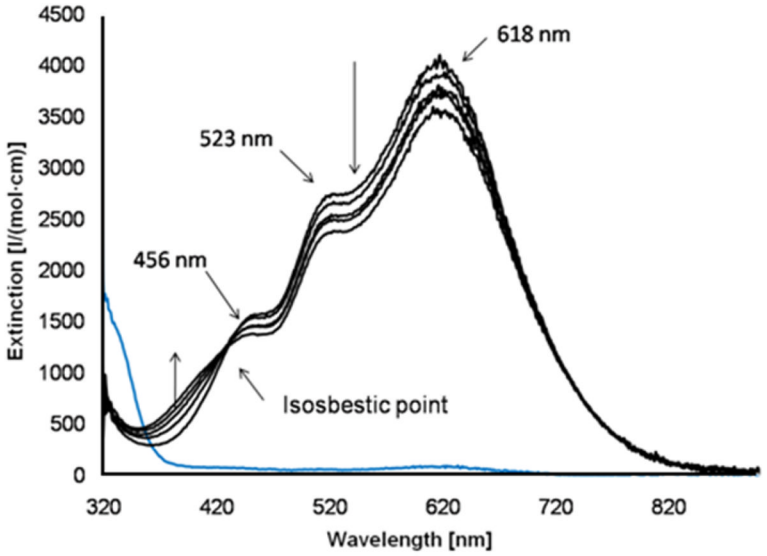

Figure 1.

Oxygenation of $[Cu^{I}(L^{1})][B(C_6F_5)_4]$ (acetone, T=−80°C, $2.5\cdot10^{-4}$M), recorded within 105 min; blue (for comparison): $[Cu^{I}(L^{1})]^{+}$; black: oxygenated complex; the values for extinction coefficients are based on 100% conversion.

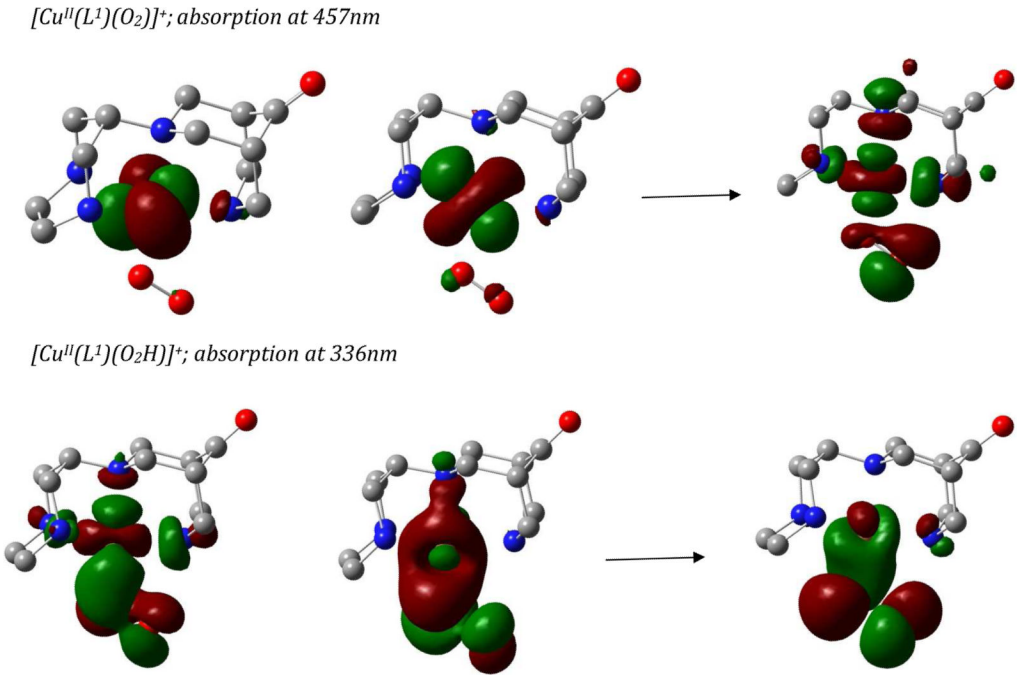

Figure 2.
Orbitals involved in the major transitions of the mononuclear complexes.

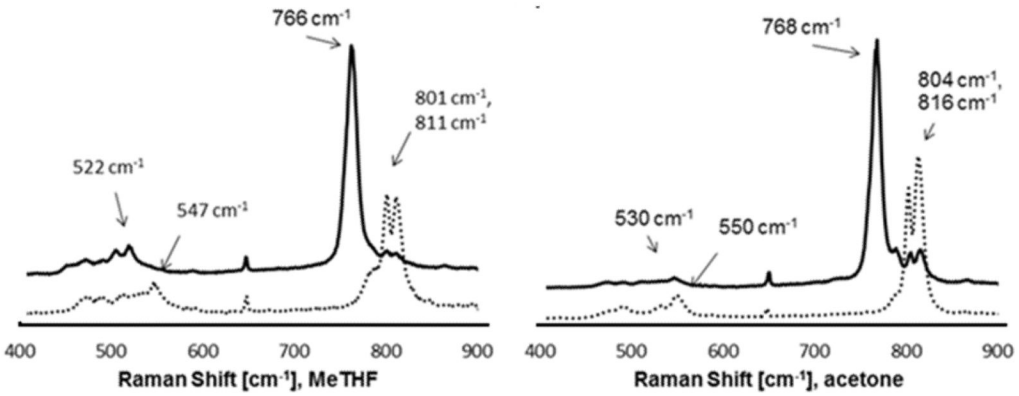

Figure 3.

Resonance Raman spectra of the product of the oxygenation of $[Cu^{I}(L^{1})]^{+}$ in MeTHF and acetone, −80°C, c=22·10^{-3}M, λ_{Laser}=623 nm; full line: $^{18}O_2$, dotted line: $^{16}O_2$.

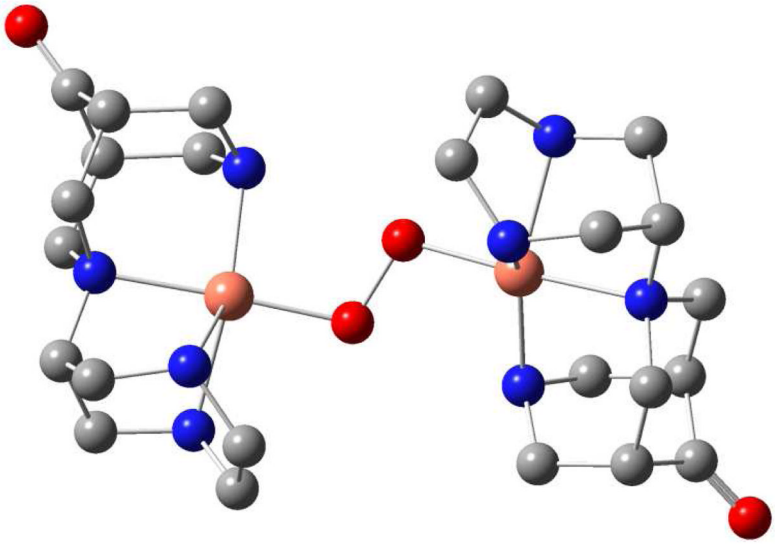

Figure 4.
Lowest energy isomer of the dinuclear *trans*-$[Cu^{II}(L^1))_2O_2]^{2+}$ complex (hydrogen atoms omitted for clarity; Cu-O: 1.94 Å; O-O: 1.52 Å, see Supporting Information for details).

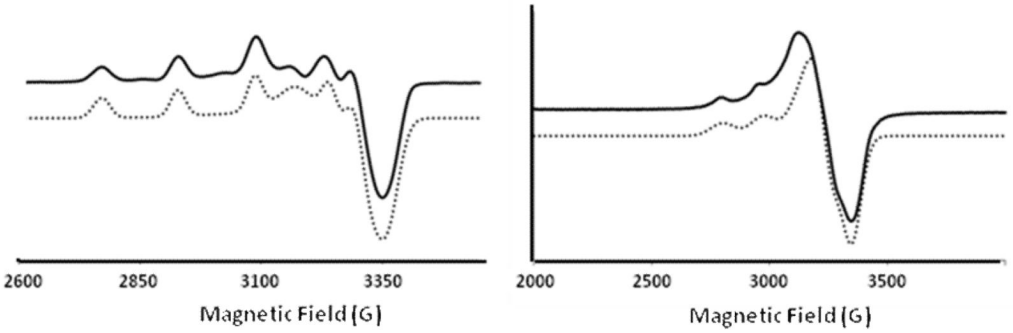

Figure 5.
EPR-Spectrum of $[Cu^{II}(L^1)O_2H]^{2+}$ (left) and $[Cu^{II}(L^1)(NCCH_3)]^{2+}$ (right); frozen solutions (90K, MeCN/toluene); continuous line: experiment, dashed line: X-Sophe[64] simulation.

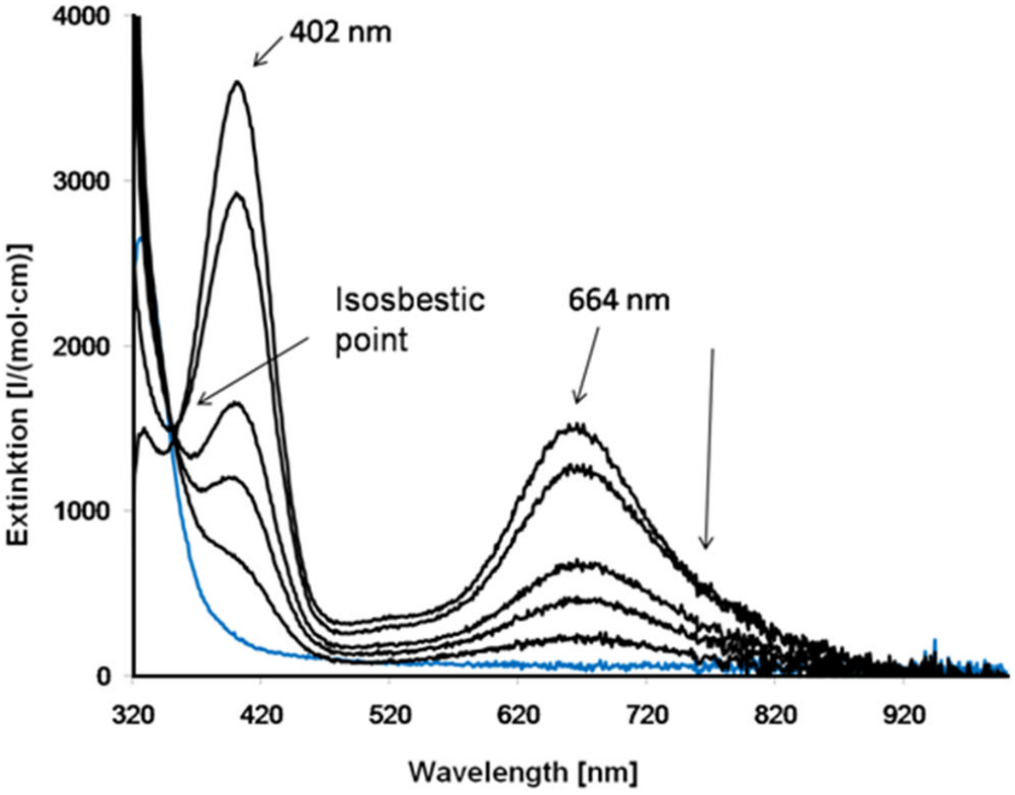

Figure 6.

Decay of $[Cu^{I}(L^{2})O_{2}]^{+}$ (acetone, saturated with O_2; −80°C; c= $5.0\cdot10^{-4}$ M), recorded over 10 min while warming up to ambient temperature; blue (for comparison): $[Cu^{I}(L^{2})]^{+}$; black: oxygenated complex; the values for extinction coefficients are based on 100% conversion of $[Cu^{I}(L^{2})]^{+} + O_2 \rightleftharpoons [Cu^{I}(L^{2})O_{2}]^{+}$.

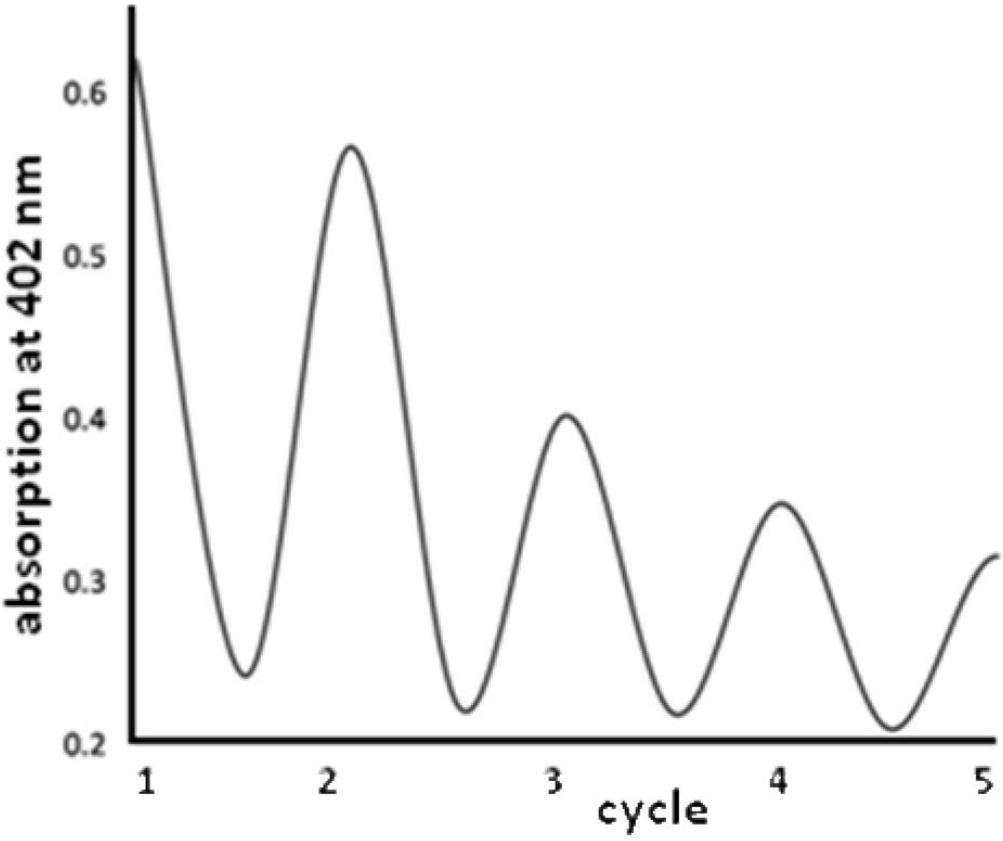

Figure 7.

Cycles of $[Cu^{I}(L^{2})O_{2}]^{+}$ (acetone, saturated with O_2; −80°C; c= $5.0 \cdot 10^{-4}$ M) with its decay product $[Cu^{I}(L^{2})]^{+}$, as a function of the temperature (closed vessel, absorption at λ = 402 nm (see Figure 7 and text); the cycles involve cooling to −80°C (maximum absorption at 402 nm) and warming to ambient temperature within approx. 30 min (minimum absorption at 402 nm).

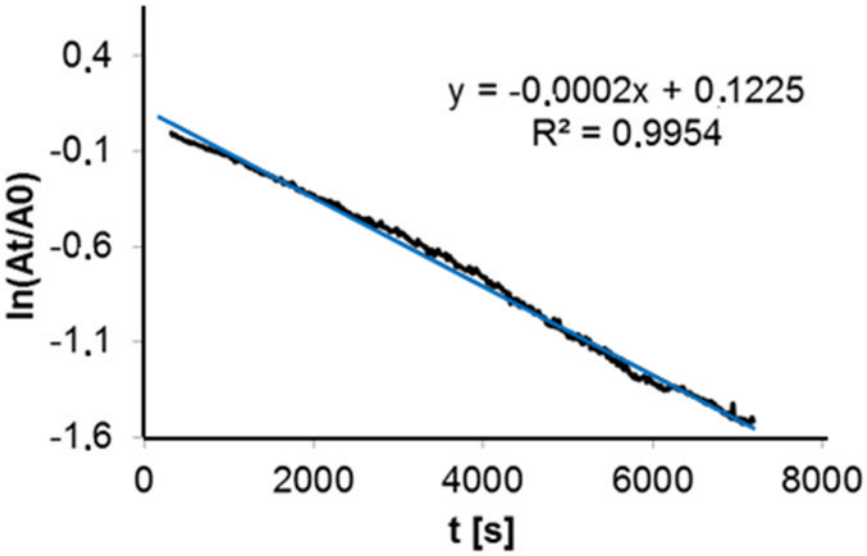

Figure 8.
Half-life ($t_{1/2}$) ln(A_t/A_0) vs. t [s]; A_0: absorption at t = 0 s; A_t: absorption at t) of $[Cu^{II}(L^2)O_2]^+$ at −35°C; THF, c = $5\cdot10^{-4}$M; λ = 408 nm.

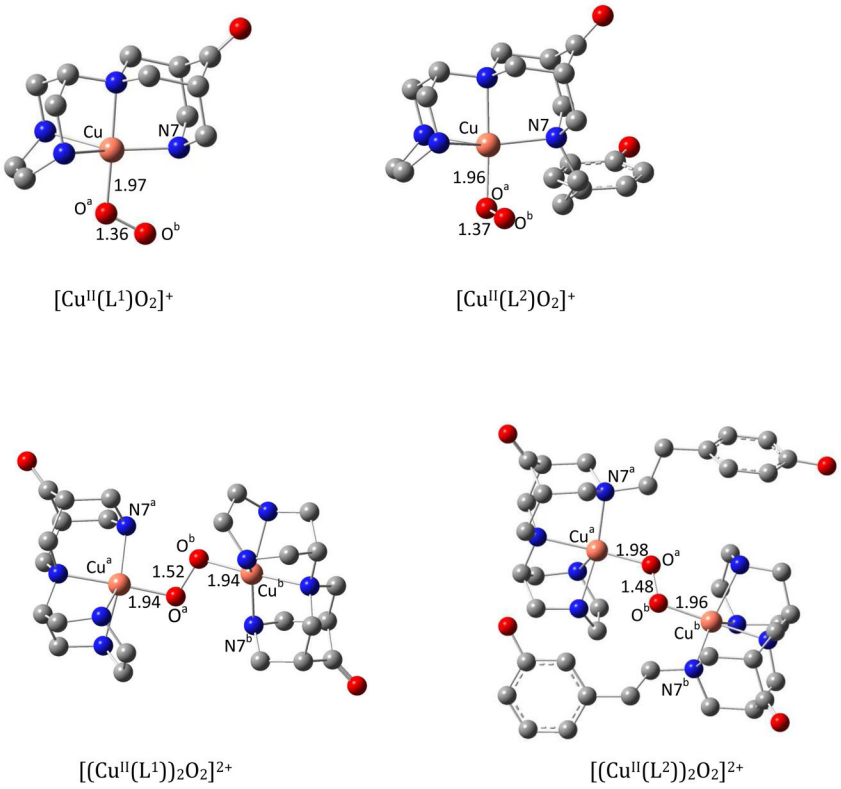

Figure 9.

DFT-optimized geometries and key structural parameters of the mono- and dinuclear copper(II)/dioxygen complexes with L^1 and L^2 (hydrogen atoms are omitted for clarity).

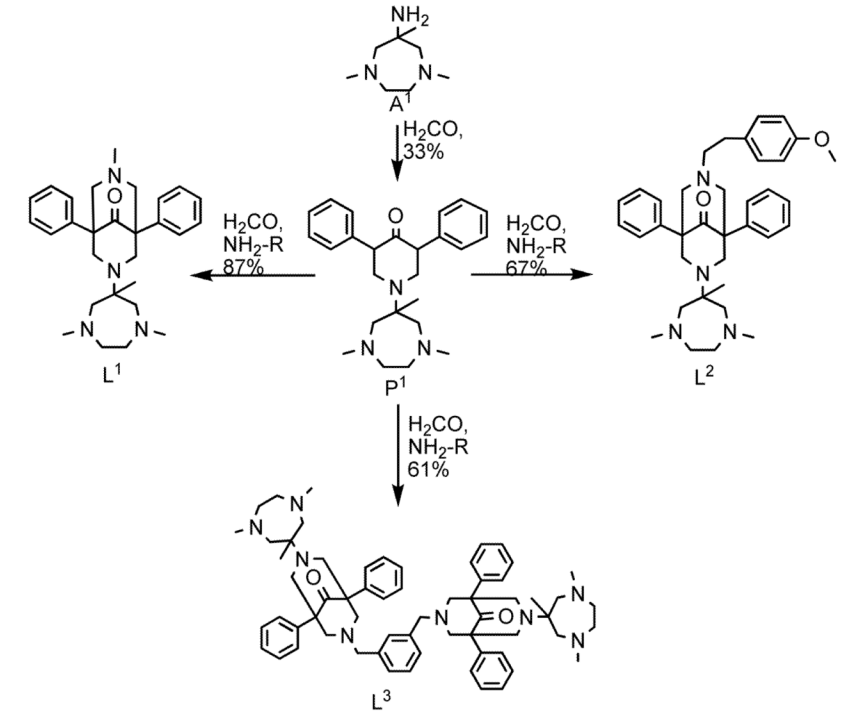

Syntheses: R=methylamine for L^1 [L^{1A} (model (i) for DFT calculations): all 3 NMe groups are replaced by NH];
R=2-(4-methoxyphenyl)ethaneamine for L^2;
R=1,3-phenylenedimethaneamine for L^2.

Scheme 1.

Syntheses and structures of the ligands L^1, L^2 and L^3.

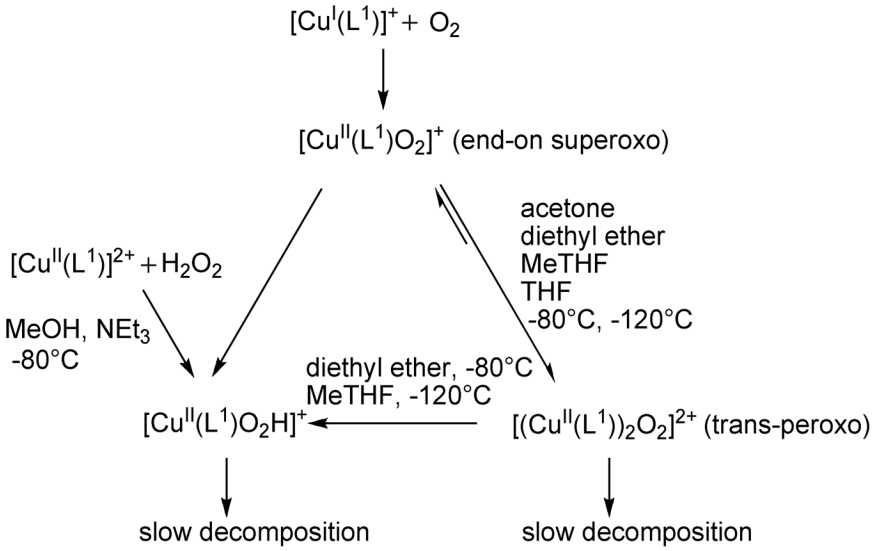

Scheme 2.
Reaction pathways for the oxygenation of $[Cu^{I}(L^{1})]^{+}$

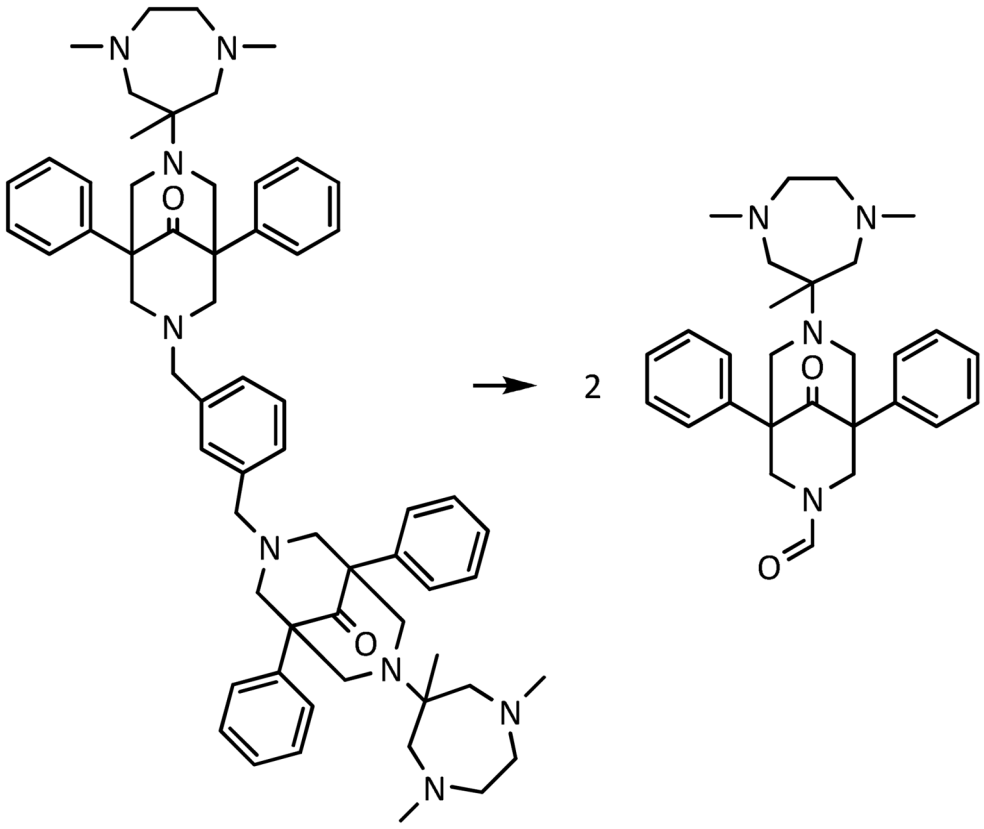

Scheme 3.
Oxidative decomposition of $[Cu^{II}_2(L^3)(O_2)_2]^{2+}$.

Table 1

EPR parameters of the Cu^{II} complexes (in MeCN/toluene or MeOH, 90K; X-band frequencies (approx. 9 GHz) the spin; Hamiltonian parameters are determined by spectral simulation with XSophe[64] (the spectra and simulations are given as Supporting Information).

complex	g_{II}	$g_{\perp}$	A_{II} [10^{-4} cm^{-1}]	$A_{\perp}$ [10^{-4} cm^{-1}]
$[Cu^{II}(L^1)(NCCH_3)]^{2+}$ [16]	2.21	2.08	170	15
$[Cu^{II}(L^2)(OH)]^{+}$	2.22	2.05	170	15

Table 2

UV-vis-NIR spectral data of the Cu^{II} complexes at ambient temperature in MeCN.

complex	λ_1[nm]/ε[l/(mol·cm)]	λ_2[nm]/ε[l/(mol·cm)]
$[Cu^{II}(L^1)(NCCH_3)]^{2+}$ [16]	903/341	627/684
$[Cu^{II}(L^2)(OH_2)]^{2+}$	--	633/136
$[Cu^{II}_2(L^3)]^{4+}$	--	599/248

Table 3

Cyclic voltammetry (CV) data of the 2nd generation bispidine-copper compounds in MeCN, 0.1 M(Bu_4N)(PF_6), $E_{1/2}$ *vs.* SCE.

complex	$E_{1/2}$ [mV]
$[Cu^{II}(L^1)(NCMe)]^{2+}$	−377
$[Cu^{II}(L^2)(OH_2)]^{2+}$	−270
$[Cu_2^{II}(L^3)(solvent)_2]^{4+}$	−396 (red), −697 (red), −555(ox)

Table 4

Key structural parameters and spin densities for various oxygenated copper complexes involving the bispidine ligand L^1 (lowest energy conformations and spin states, where appropriate, see text).

complex	interatomic distances [Å]			spin densities		
	Cu-O	O-O	Cu-N_{avg}	Cu	O	O
$[(Cu^{II}(L^{1A}))_2O_2]^{2+}$	1.938 1.939	1.516	2.193	0.49 −0.49	0.18	−0.18
$[Cu^{II}(L^1)(O_2)]^+$	1.970	1.360	2.147	0.45	0.17	−0.55
$[Cu^{II}(L^1)(O_2H)]^+$	1.911	1.530	2.403	0.50	0.22	−0.01

Table 5

Experimental and calculated resonance Raman transitions of the oxygenation product of $[Cu^{I}(L^{1})]^{+}$ at −80°C (computed values not scaled, see text).

solvent	O-O, $^{16}O_2$, [cm^{-1}]	Cu-O, $^{16}O_2$, [cm^{-1}]	O-O, $^{18}O_2$, [cm^{-1}]	Cu-O, $^{18}O_2$, [cm^{-1}]	Δ (O-O), [cm^{-1}]	Δ (Cu-O), [cm^{-1}]
MeTHF	811, 801	547	766	522	45, 35	25
acetone	816, 804	550	768	530	48, 36	20
calculated	808, 798	495	--	--	--	--

Table 6

Spin Hamiltonian parameters of the experimental EPR spectra (X-band frequencies, X-Sophe[64] simulation, see Figure 6) (and calculated parameters; DFT, see text) of $[Cu^{II}(L^1)(O_2H)]^{2+}$ and $[Cu^{II}(L^1)(NCCH_3)]^{2+}$.

complex	g_x	g_y	g_z	A_x [$10^{-4}cm^{-1}$]	A_y [$10^{-4}cm^{-1}$]	A_z [$10^{-4}cm^{-1}$]
$[Cu^{II}(L^1)O_2H]^+$	2.034 (2.026)	2.074 (2.065)	2.232 (2.137)	31 (27)	33 (33)	162 (168)
$[Cu^{II}(L^1)(NCCH_3)]^{2+}$	2.08 (2.06)	= g_x	2.21 (2.27)	15 (30)	= A_x	170 (172)